Three-dimensional structure of *P*-wave anisotropy beneath the Tohoku district, northeast Japan

Motoko Ishise and Hitoshi Oda

Department of Earth Sciences, Okayama University, Okayama, Japan

Received 24 December 2004; revised 26 March 2005; accepted 8 April 2005; published 20 July 2005.

[1] We retrieve three-dimensional structures of isotropic and anisotropic velocities of P-waves of the Tohoku district from first P-arrival time data, assuming azimuthal anisotropy to be caused by hexagonal symmetry axes distributed horizontally in the Earth. The results show that the high-velocity Pacific slab is clearly imaged in the isotropic velocity structure, even though the azimuthal anisotropy is taken into account. In addition, small-scale low-velocity regions and prominent low-velocity anomalies are found just below the active volcanoes and in the mantle wedge above the high-velocity Pacific slab, respectively. The fast propagation axis of P-waves is in mostly E-W direction in the upper crust, nearly N-S and E-W directions in the lower crust, E-W direction in the mantle wedge, and N-S direction in the descending Pacific slab. These features of the P-wave anisotropy structure are consistent with those of lateral variations of the fast polarization directions measured previously by shear-wave splitting observations. The plausible factor that causes the crust anisotropy is interpreted as being alignment or preferred orientation of microcracks and crust minerals. The mantle wedge anisotropy is attributed to lattice preferred orientation of the mantle minerals arising from present-day mantle process such as the mantle wedge convection and the plate motion. However, the fast propagation axis of P-waves in the slab is almost perpendicular to the magnetic lineation of the oceanic plate under the northwest Pacific, and thus the slab preserves the original anisotropic property that the Pacific plate gained when it formed.

Citation: Ishise, M., and H. Oda (2005), Three-dimensional structure of *P*-wave anisotropy beneath the Tohoku district, northeast Japan, *J. Geophys. Res.*, *110*, B07304, doi:10.1029/2004JB003599.

1. Introduction

[2] Three-dimensional (3-D) structures of isotropic seismic velocities revealed a high-velocity oceanic slab descending beneath the northeast Japan island arc and some intensive low-velocity anomaly regions in the mantle wedge above the slab [e.g., *Hasemi et al.*, 1984; *Zhao et al.*, 1992; *Nakajima et al.*, 2001]. Such tomographic studies of the seismic velocity structure help us comprehend the Earth's material transfer arising from the mantle wedge convection and plate motion. Another approach to know the material transfer in the Earth is given by seismic anisotropy. Laboratory experiments indicated that the upper mantle anisotropy is governed by alignment of mantle minerals and partially melted inclusions in the direction of the convective mantle flow and the crust anisotropy is caused by microcrack alignment in the horizontal principal axes of local stress field in the crust [*Nur and Simmons*, 1969; *McKenzie*, 1979; *Karato and Wu*, 1993; *Zhang and Karato*, 1995]. Therefore the seismic anisotropy is important to understand the mantle dynamics and tectonics of the Earth's interior.

[3] The effect of seismic anisotropy appears on the seismogram in various forms, for example, azimuthal dependence of P-wave velocity [*Raitt et al.*, 1969], shear-wave splitting [*Crampin*, 1978], surface-wave polarization anomaly caused by coupling between Rayleigh and Love waves [*Kirkwood and Crampin*, 1981], and Rayleigh-Love wave discrepancy where the Love wave phase velocity is not consistent with that predicted from isotropic velocity model obtained by inversion of the Rayleigh wave dispersion data [*Cara and Leveque*, 1988]. These phenomena have been utilized to investigate the seismic anisotropy at various depths in the Earth. In particular, the shear-wave splitting method has been employed for the studies of regional variation in S-wave anisotropy [e.g., *Ando et al.*, 1980, 1983; *Kaneshima*, 1990; *Okada et al.*, 1995; *Oda and Shimizu*, 1997; *Hiramatsu et al.*, 1998; *Wolfe and Solomon*, 1998; *Audoine et al.*, 2000; *Fischer et al.*, 2000; *Nakajima and Hasegawa*, 2004]. Consequently, the fast polarization direction of split shear wave proved to be parallel to the maximum compression axis in the crust and to agree with subduction direction of the oceanic slab in the upper mantle [*Kaneshima*, 1990; *Savage*, 1999; *Okada et al.*, 1995; *Wolfe*

0148-0227/05/2004JB003599$09.00

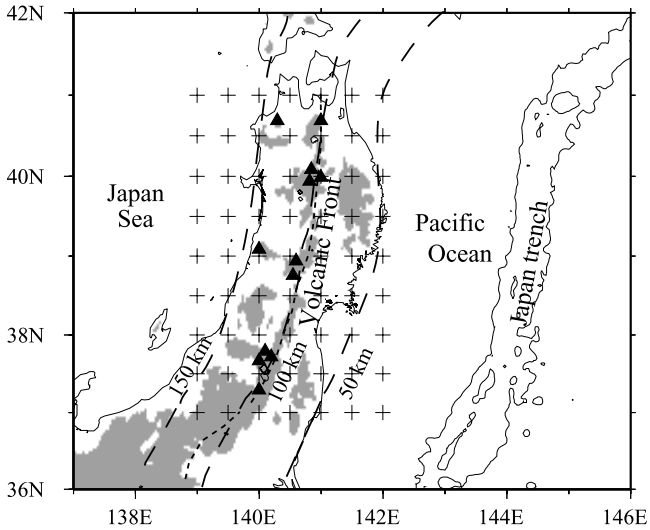

Figure 1. Map of the Tohoku district, northeast Japan. Gray areas represent the mountain regions of altitude higher than 500 m. Triangles indicate the representative active volcanoes and the dotted line shows the volcanic front. Isodepth contours of deep-focus earthquakes are shown at 50-km intervals by dashed lines. The small crosses show nodes of horizontal grid net. The nets are set at nine depths (0, 10, 25, 40, 55, 70, 100, 130, and 160 km).

and Solomon, 1998; *Audoine et al.*, 2000; *Fischer et al.*, 2000]. Furthermore the seismic anisotropy was also detected in the oceanic plate lying under the ocean floor [e.g., *Shimamura*, 1984] and in the oceanic slab subducting beneath the Japan islands [*Fukao*, 1984; *Hiramatsu et al.*, 1997], but there is almost no study on spatial variation of the seismic anisotropy in the descending oceanic slab.

[4] The shear-wave splitting is available for diagnosis that there is anisotropic zone somewhere on a ray path of shear wave, but has poor ability to specify what zone on the ray path is anisotropic. Moreover, the application is restricted to only the shear waves propagating along nearly vertical ray path, and thus the polarization anomaly data have poor resolution to estimate the vertical variation of S-wave anisotropy. These situations prevent us from retrieving 3-D anisotropic structure from the shear-wave splitting data, although the polarization anomaly measurements at denser stations make it possible to reveal the regional variation of S-wave anisotropy. In contrast to the shear-wave splitting, the P-wave travel time data are thought to have high resolution to image lateral variations of isotropic and anisotropic velocity structures. Recently, *Ishise and Oda* [2002] presented a seismic tomography method incorporating lateral variations of isotropic and anisotropic velocity structures, modifying the method developed by *Hirahara and Ishikawa* [1984]. A similar tomography technique was developed to infer lateral variation of the fast propagation direction of P-waves [*Hearn*, 1996; *Chen et al.*, 2003; *Eberhart-Phillips and Henderson*, 2004]. In particular, *Eberhart-Phillips and Henderson* [2004] improved *Hearn*'s [1996] technique that determines simultaneously both two-dimensionally varying velocity and azimuthal anisotropy from P_n travel time data, and estimated 3-D structure of isotropic and anisotropic velocity by analyzing P-wave travel time data through the improved Hearn's technique. Our method used in this study is similar to their method with respect to methodology to retrieve isotropic velocity and azimuthal anisotropy from P-wave travel time data. Difference between the two methods is that in our method simple initial models of one dimension are used and damping factor is determined by trial and error, whereas Eberhart-Phillips and Henderson's method used informative initial models incorporating lateral heterogeneity of the velocity structure and shear-wave splitting data and employed a skillful technique to determine damping factor.

[5] The main objective of this study is to image 3-D variation of isotropic and anisotropic velocity structures of the Tohoku district, northeast Japan island arc, where the old Pacific plate formed 130 Myr ago [*Sclater et al.*, 1981] is subducting toward the west from the Japan trench. In section 2, we review the modified tomographic method to retrieve both the isotropic and anisotropic velocity structures from the first P-arrival time data. In section 3, we explain the P-arrival time data, local earthquake hypocenters and one-dimensional velocity structure used as initial velocity model for the travel time inversion. In sections 4, the 3-D velocity structures obtained and their features are presented. In section 5, we discuss plausible factors that cause the seismic anisotropy in the crust, mantle wedge and the Pacific slab and examine the validity of our estimates of the seismic anisotropy structure, comparing with the results of the explosion seismological experiments, the geomagnetic study of ocean bottom and other seismological studies.

2. Method

[6] The elastic anisotropy of olivine-rich peridotites, a major candidate of the upper mantle material, is approximately represented as hexagonal anisotropy [*Christensen*, 1984; *Park and Yu*, 1992]. In the case of weak azimuthal anisotropy which is caused by the hexagonal symmetry axes distributed horizontally in the Earth, the P-wave velocity perturbation is approximated as the equation [*Backus*, 1965; *Hirahara and Ishikawa*, 1984],

$$\frac{\Delta v}{v_0} = A + B(\sin i)^2\{1 + \cos 2(\phi - \theta)\}. \quad (1)$$

Derivation of the equation is shown in Appendix A. In (1), A is the dimensionless perturbation to a reference isotropic velocity v_0, B and θ are the anisotropic parameters to describe the anisotropy intensity and the azimuth of the hexagonal symmetry axis, respectively, ϕ is the azimuth of the ray path, and i is the angle measured from the upward vertical axis to the ray path. The first and second terms of (1) represent the dimensionless perturbations of isotropic and anisotropic velocities, respectively. In general, the travel time of P-wave propagating into an elastic medium with isotropic and anisotropic heterogeneity should be calculated using the algorithm developed by *Cerveny* [1972] and *Shearer and Champman* [1988], but the assumption of weak anisotropy allows us to employ two-point ray tracing

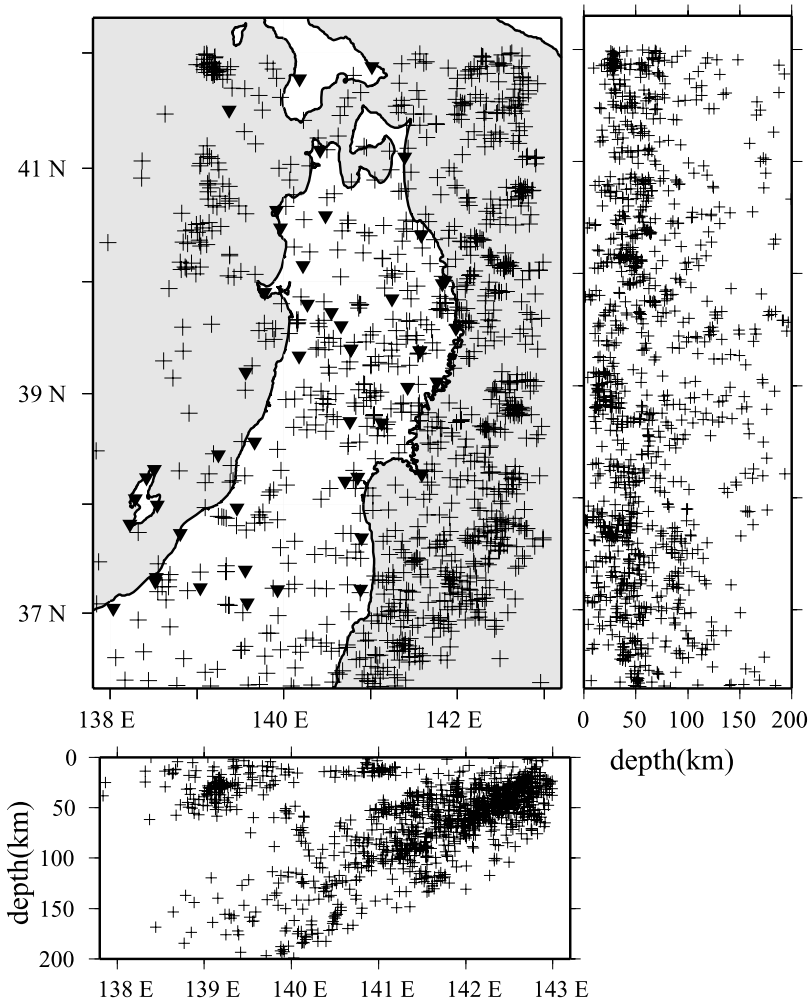

Figure 2. Locations of the original earthquake hypocenters (crosses) and stations (triangles) taken from JUNEC.

algorithm, which was developed for the travel time calculation of a laterally heterogeneous isotropic velocity structure [*Um and Thurber*, 1987]. When a ray path made of N segments is determined by the algorithm, the P-wave travel time is calculated by

$$t = \sum_{q=1}^{N} \frac{l_q}{V_q}, \tag{2}$$

where l_q is the length of the qth segment, and V_q denotes the velocity at the midpoint of the segment, as defined by

$$V_q = v_q + b_q(\sin i_q)^2\{1 + \cos 2(\phi_q - \theta_q)\}, \tag{3}$$

where $v_q = v_0(1 + A_q)$ and $b_q = v_0 B_q$.

[7] We set a Cartesian grid system to model 3-D velocity structure, which is parameterized by specifying the velocity parameters, v, b and θ, on all the grid nodes. To calculate the travel time in the heterogeneous velocity structure by making use of (2), we must know the velocity V_q on the midpoints of N segments constituting a ray path. The velocity parameters, v, b and θ, at a coordinate (x, y, z), which are denoted by $f(x, y, z)$, are evaluated by interpolation formula [*Thurber*, 1983]

$$f(x,y,z) = \sum_{i=1}^{2}\sum_{j=1}^{2}\sum_{k=1}^{2} w_{ijk}(x,y,z) f(x_i, y_j, z_k), \tag{4}$$

where $f(x_i, y_j, z_k)$ is the parameter on the coordinates (x_i, y_j, z_k; i, j, k = 1, 2) of the eight grid nodes surrounding the given point (x, y, z), and the weight function is defined as

$$w_{ijk}(x,y,z) = \left(1 - \left|\frac{x - x_i}{x_2 - x_1}\right|\right)\left(1 - \left|\frac{y - y_j}{y_2 - y_1}\right|\right)\left(1 - \left|\frac{z - z_k}{z_2 - z_1}\right|\right). \tag{5}$$

[8] Theoretical travel times are calculated for a given 3-D velocity structure by making use of (2) with the aid of interpolation formula (4). The residual Δt between observed and calculated arrival times is linearized in terms of velocity parameter changes, Δv_q, Δb_q and $\Delta\theta_q$, and source parameter

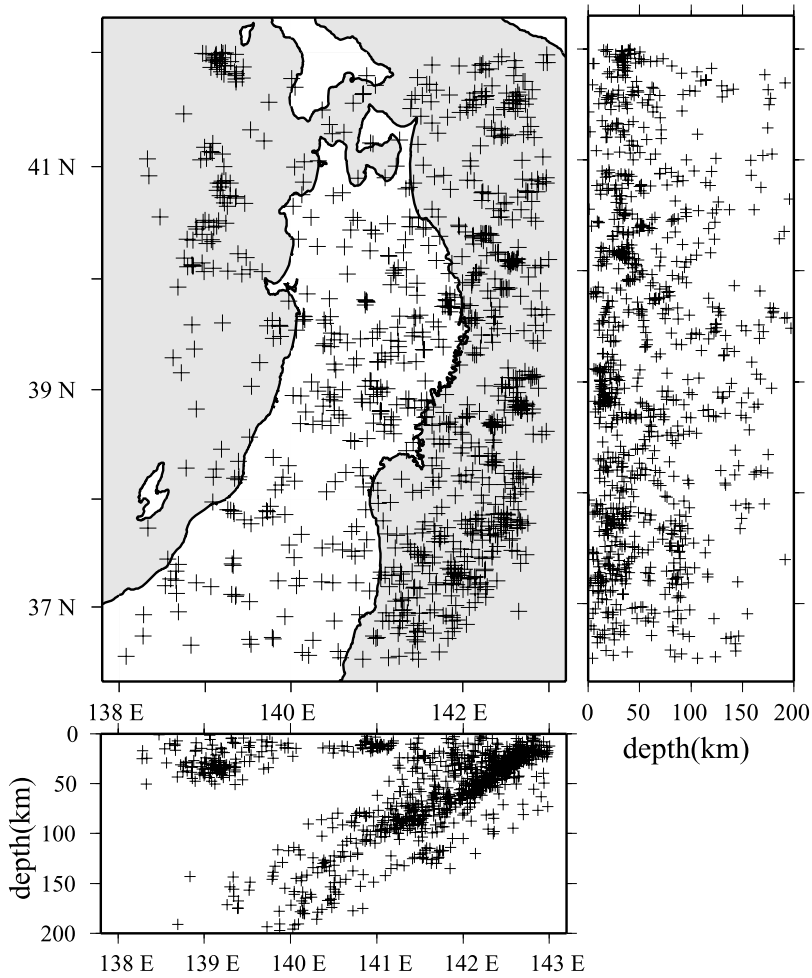

Figure 3. Locations of the relocated earthquake hypocenters.

changes of hypocenter coordinates and origin time, Δs_i (i = 1, 2, 3, 4)

$$\Delta t = \sum_{q=1}^{N} \left\{ \left(\frac{\partial t}{\partial v_q}\right)\Delta v_q + \left(\frac{\partial t}{\partial b_q}\right)\Delta b_q + \left(\frac{\partial t}{\partial \theta_q}\right)\Delta \theta_q \right\} + \sum_{i=1}^{4} \frac{\partial t}{\partial s_i}\Delta s_i. \tag{6}$$

The first parenthesized term is the contribution from the velocity parameter changes and the second term is from the source parameter changes. The partial derivatives are calculated by

$$\begin{aligned} \frac{\partial t}{\partial v_q} &= -\frac{l_q}{V_q^2} \\ \frac{\partial t}{\partial b_q} &= -\left(\frac{l_q}{V_q^2}\right)(\sin i_q)^2\{1+\cos 2(\phi_q-\theta_q)\} \\ \frac{\partial t}{\partial \theta_q} &= -2\left(\frac{l_q}{V_q^2}\right) b_q (\sin i_q)^2 \sin 2(\phi_q-\theta_q) \end{aligned} \tag{7}$$

and the derivatives $\dfrac{\partial t}{\partial s_i}$ with respect to source parameters are also known [e.g., *Thurber*, 1983]. Since the small changes, Δv_q, Δb_q and $\Delta\theta_q$, at a coordinate (x, y, z) are also expressed similarly to (4), (6) is rewritten in terms of the velocity

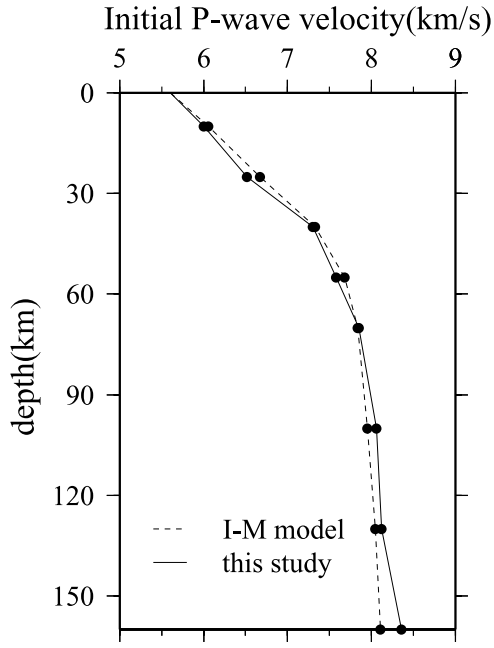

Figure 4. Ichikawa-Mochizuki's velocity model (I-M model) and one-dimensional velocity model estimated from the first P-arrival time data.

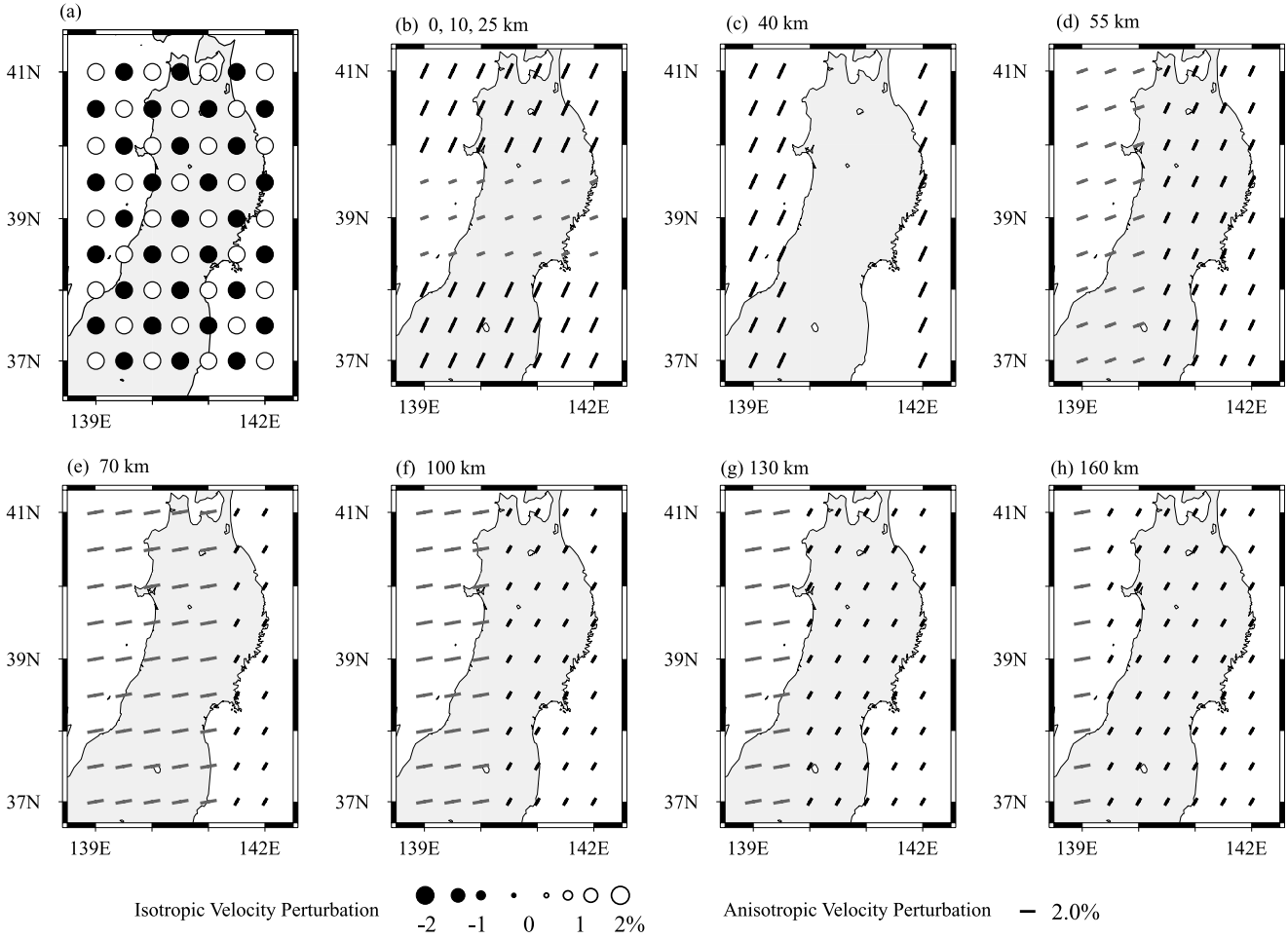

Figure 5. Isotropic and anisotropic velocity perturbations of P-waves used to produce the synthetic P-travel time data. (a) Lateral variations of 2% isotropic velocity perturbations at 0-, 25-, 55-, 100-, and 160-km depths. The lateral variations of the velocity perturbations at 10-, 40-, 70-, and 130-km depths are represented as the reverse pattern to Figure 5a. Open and solid circles denote high- and low-velocity perturbations, respectively. (b–h) Lateral variations of azimuthal anisotropy are shown, to each of which the depth is assigned. Azimuth and length of bars represent the fast propagation direction of P-wave and anisotropy intensity. Gray and black bars indicate the fast propagation axes orientating from N45°E–S45°W to S45°E–N45°W and from N45°W–S45°E to N45°E–S45°W, respectively. The perturbation scales are shown in the bottom.

perturbations, Δv_k, Δb_k and $\Delta\theta_k$, at M grid nodes surrounding the given ray path

$$\Delta t = \sum_{k=1}^{M} (\alpha_k \Delta v_k + \beta_k \Delta b_k + \gamma_k \Delta\theta_k) + \sum_{i=1}^{4} \frac{\partial t}{\partial s_i} \Delta s_i, \qquad (8)$$

where the coefficients α_k, β_k and γ_k are calculated using the partial derivatives of (7). The equations (8) relating the arrival time residuals to the model parameter changes are obtained for a number of station-event pairs, so we can estimate the isotropic and anisotropic velocity perturbations, Δv_k, Δb_k and $\Delta\theta_k$ and the source correction terms $\Delta s_i (i = 1, 2, 3, 4)$, solving the equations by the damped least squares method. The velocity parameters, v_k, b_k and θ_k, and the source parameters are determined by adding the least squares solution to the given initial parameters. Unfortunately the simultaneous determination of the velocity and source parameters sometimes yields an unstable solution that is geophysically meaningless. This situation may be avoided by using smoothing constraints for isotropic velocity model and other constraints for anisotropy parameters, as a priori shear-wave splitting anisotropy model, but the solution may be dependent on the given initial model parameters and the constraints. Another way to obtain the reasonable solution is to determine the velocity and source parameters alternately. This alternating solution approach has been shown to produce solution bias [*Thurber*, 1992], but the bias is confirmed to be not large, as will be shown by numerical experiments in the next section. Thus, in this study, we employ the latter method, i.e., after relocating earthquake hypocenters the velocity parameters are determined using the relocated earthquake hypocenters, and then the source parameters are improved using the estimated velocity model. The inversion procedure is

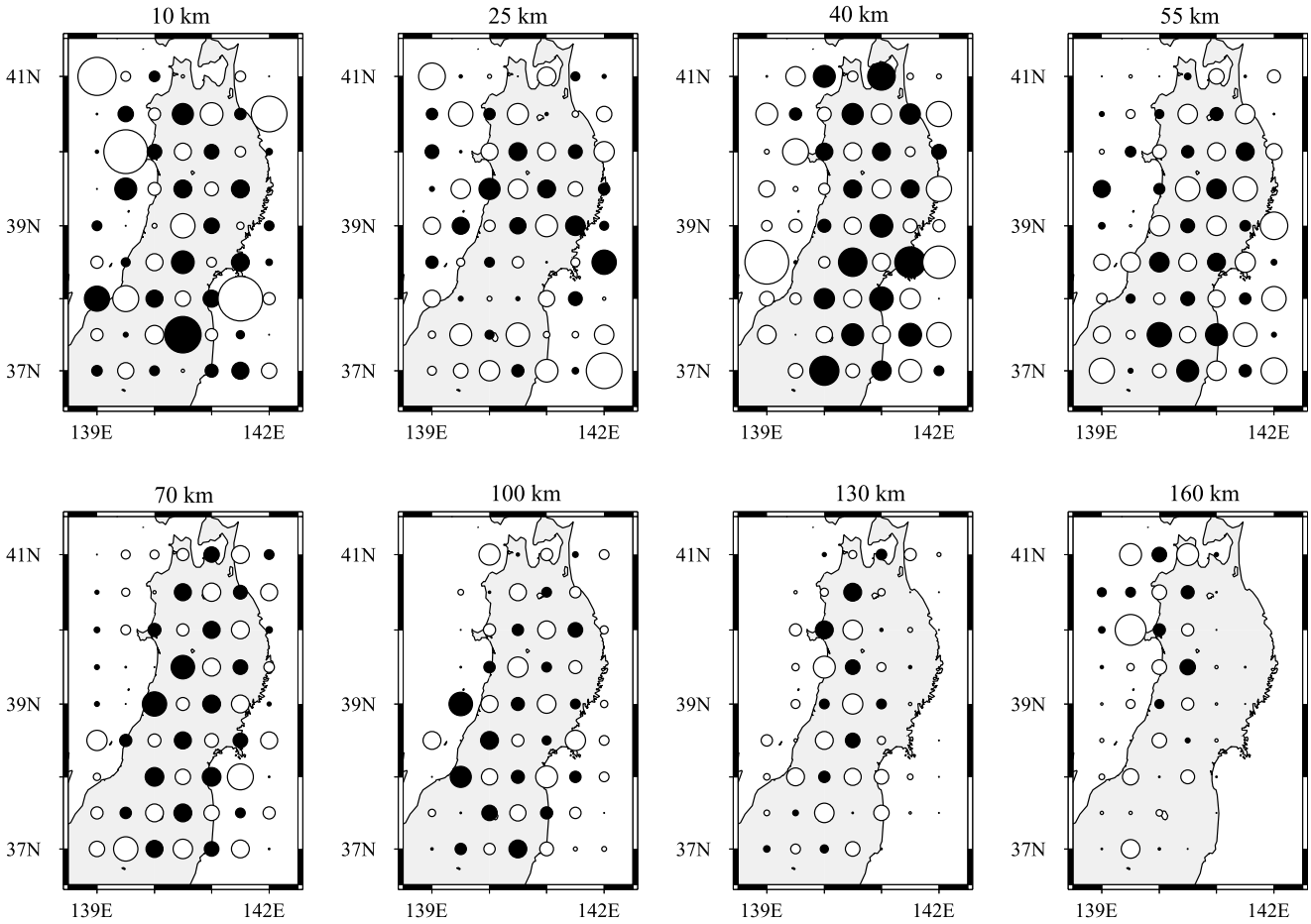

Figure 6. Map of isotropic velocity perturbations estimated from the error-free travel time data. See Figure 5 for symbols and perturbation scale.

repeated until rms of P-wave arrival time residuals is below a threshold level. The final 3-D velocity structure obtained through the inversion calculation is visualized by mapping the velocity parameter values on the grid nodes.

3. Seismological Data and Initial Velocity Model

[9] The study area is in the latitude range of 36–42°N and the longitude range of 138–143°E of the Tohoku district (Figure 1). A Cartesian grid system is also shown in Figure 1, where the grid nodes are horizontally spaced every 0.5° at nine depths (0, 10, 25, 40, 55, 70, 100, 130, 160 km). We choose 47 stations of the Japan University Network and select 961 local earthquakes which meet the following conditions: (1) the focal depth is less than 230 km, (2) the first P arrival is clearly observed at more than 5 stations, and (3) the earthquake epicenter is located in the study area. The data of source parameters and first P-arrival time are taken from the Japan University Network Earthquake Catalogue (JUNEC) in 1994. We discarded the arrival time data earlier or later than theoretical travel times by 3.0 s or more. Consequently about 15,000 arrival time data are adopted. Locations of the stations and earthquake hypocenters are shown in Figure 2.

[10] The source parameters listed in JUNEC are determined using Ichikawa-Mochizuki's model [*Ichikawa and Mochizuki*, 1971; *Hamada*, 1984] by the Earthquake Information Center (EIC) of the Earthquake Research Institute, based on P- and S-wave arrival times that are measured by local seismic networks of Japanese national universities. Since the upper mantle structure beneath the Tohoku district may be significantly heterogeneous because of the massive oceanic slab and complex mantle wedge convection, a velocity model optimized so as to match the travel time data should be employed as an initial model for 3-D travel time inversion. For this reason, we redetermine both hypocenter locations and one-dimensional P-wave velocity model from the P-arrival time data. The relocated hypocenters and one-dimensional velocity structure are shown in Figures 3 and 4, respectively. The differences between the relocated and original hypocenters are less than several kilometers. The double seismic zone of deep earthquakes can be more clearly identified in the relocated hypocenter distribution (Figure 3) than in the original hypocenter distribution (Figure 2). The redetermined velocity model almost agrees with Ichikawa-Mochizuki's model, but the P-wave velocity is somewhat higher in the depth interval of 100–160 km. We use the one-dimensional velocity model as initial model for isotropic velocity structure, along with the relocated earthquake hypocenters. It should be noted that a high-velocity oceanic slab is not assumed in the initial velocity model. As initial

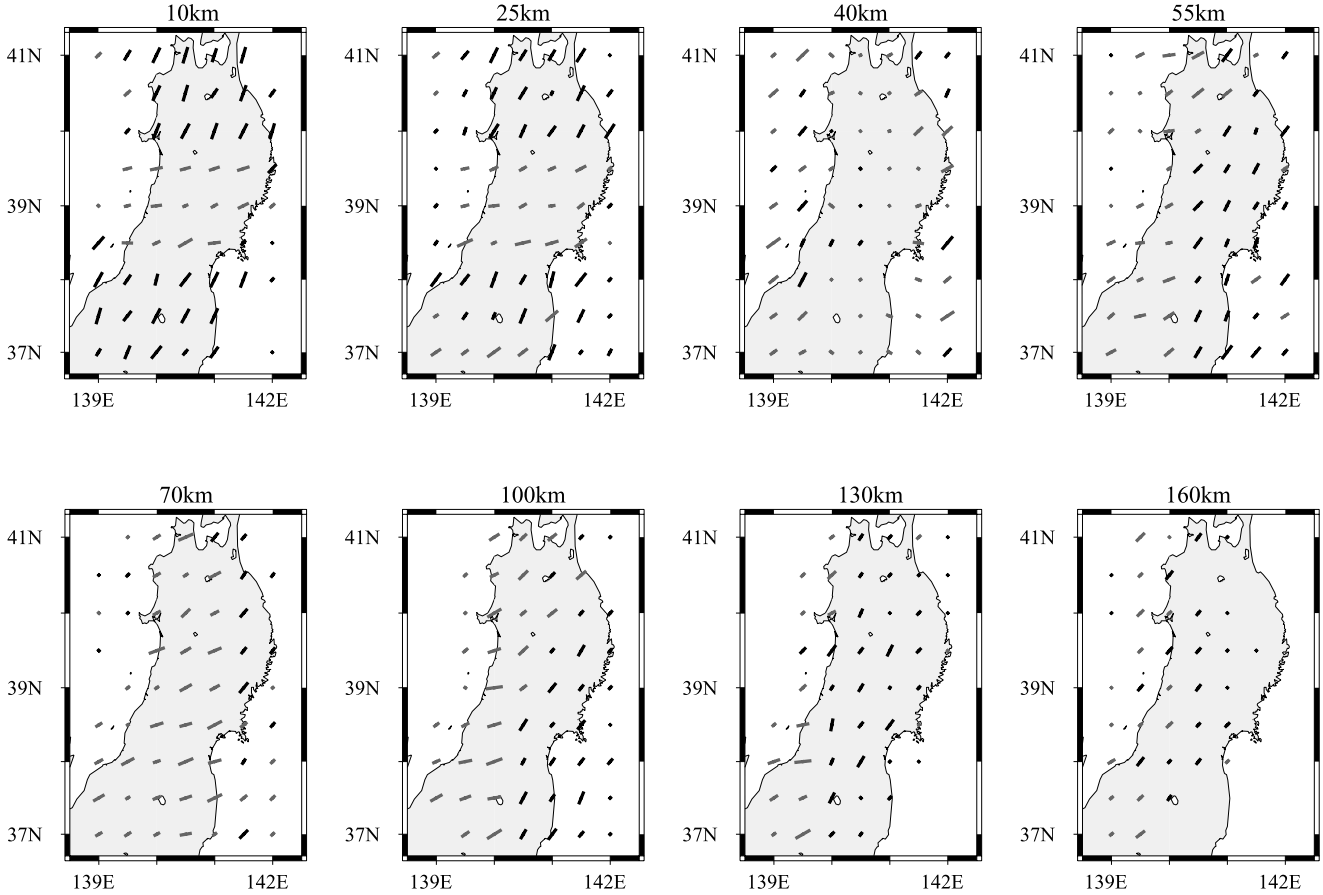

Figure 7. Map of anisotropic velocity perturbations estimated from the error-free travel time data. See Figure 5 for symbols and perturbation scale.

model for anisotropy structure, we employ another model in which the hexagonal symmetry axes with 0.001% anisotropy intensity are uniformly distributed in E-W direction.

4. Results

4.1. Numerical Experiments

[11] Before analyzing the real data, in order to examine the validity of our inversion method we implement two numerical tests using the P-arrival time data which are synthesized for the real source-station pairs. For this purpose, we prepare two sets of synthetic data; one is composed of error-free P-arrival time data and the other is made of the data contaminated with random errors of 0.05s standard deviation. Figure 5 depicts isotropic and anisotropic velocity structures for which the synthetic arrival time data are produced. The heterogeneity of isotropic velocity is represented by checker board pattern of ±2% velocity anomaly, and the heterogeneity of anisotropic velocity is shown by bars, the length and azimuth of which indicate the intensity and fast propagation direction of azimuthal anisotropy, respectively. The magnitudes of the anisotropy intensity are smaller than 3.0%, which is the same order of magnitude as the isotropic velocity heterogeneity. Table 1 shows the average and standard deviation of the differences between the relocated hypocenters and the given hypocenters to produce the synthetic data. Average absolute values of hypocenter mislocations and origin times are smaller than 0.6 km and 0.2 s, as shown in Table 1. The source parameter changes are thought to be not large enough to have significant effect on estimate of laterally heterogeneous patterns of isotropic and anisotropic velocity perturbations. The velocity structures obtained are shown in Figures 6 and 7 for the error-free data and in Figures 8 and 9 for the error-contaminated data. Good recovery is achieved for laterally heterogeneous patterns of the isotropic and anisotropic velocity perturbations, but the magnitudes of the velocity heterogeneity and anisotropy are poorly recovered. The poor recovery of the velocity perturbation magnitudes and the hypocenter mislocations may be due to the solution bias which our alternating solution approach to solve (8) gives rise to, as *Thurber* [1992] pointed out. It should be noted that the area of zero percent anisotropy given at 40 km depth is imaged as an area of weak anisotropy. We find no clear trade-off between the isotropic velocity perturbation and anisotropy intensity. These results of numerical experiments demonstrate that our inversion method is able to retrieve 3-D isotropic and anisotropic velocity structure from P-arrival time data.

4.2. Real Inversion

[12] The real P-arrival time data are inverted for 3-D isotropic and anisotropic velocity structure, along with

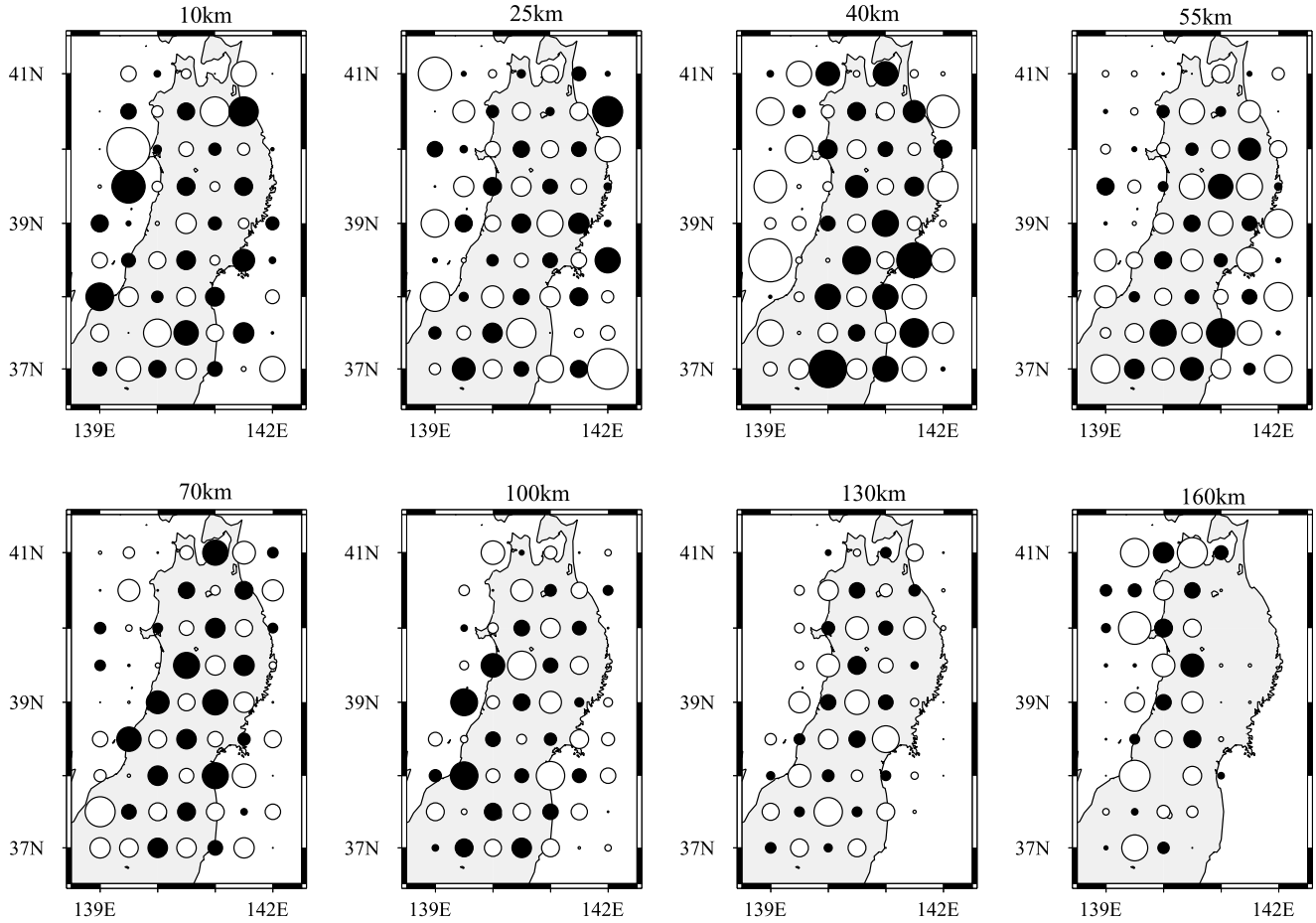

Figure 8. Map of isotropic velocity perturbations estimated from the error-contaminated travel time data. See Figure 5 for symbols and perturbation scale.

source parameters. Figure 10 depicts the lateral variations of isotropic P-wave velocity at different depths. Some small-scale low-velocity anomaly regions near the active volcanoes are characteristic of lateral heterogeneity of isotropic velocity above 40 km depth. A high-velocity region begins to appear at 55 km depth under the east coast of the Tohoku district. It shifts toward the west with increasing depth and is traced down to about 130 km depth under the west coast. Intensive low-velocity anomaly regions at the depth of 55–130 km are in contact with the western side of the high-velocity region extending parallel to the volcanic front. The boundary between the high- and low-velocity anomaly regions is nearly parallel to the strike of the isodepth contour of the deep-focus earthquakes (Figure 1). Figure 11 shows vertical cross sections of the isotropic velocity structure along A–A′ and B–B′ lines across the northeast Japan arc. Each cross section reveals a slab-like high-velocity anomaly body subducting below the low-velocity anomaly region. The high-velocity region almost coincides with the deep-focus and intermediate-depth seismic zone. Similar results were reported by the tomography studies in the Tohoku district [*Zhao et al.*, 1992; *Zhao and Hasegawa*, 1993; *Nakajima et al.*, 2001]. The slab-like high-velocity anomaly region is the Pacific slab subducting into the upper mantle and the low-velocity anomaly region above the slab reflects the ascending flow of hot mantle material in the mantle wedge and the source to supply magma to active volcanoes. It is interesting that the high-velocity Pacific slab is imaged as clear high-velocity body, even though a laterally homogeneous velocity model is used as an initial model and the seismic anisotropy is taken into account. Similarly, *Zhang et al.* [2004] reported that the Pacific slab was imaged by the travel time inversion using an initial velocity model with no plate boundary.

[13] Lateral variations in anisotropy structure at different depths are shown in Figure 12, where bar indicates the fast propagation axis of P-waves and its length is proportional to the anisotropy intensity. The fast propagation axis orientating from N45°W–S45°E to N45°E–S45°W is shown by blue bar, and the other axis orientation is shown by red bar. The anisotropy intensity in the crust and upper mantle is less than 3%. The distribution of the axis orientation systematically varies with increasing depth. The E-W axis orientation is predominant in the vicinity of the ground surface (see Figure 14). In the crust at 10 and 25 km depths, the fast propagation axes in nearly E-W direction are marked in the forearc side, the east side of the volcanic front, and the N-S axis orientation appears dominantly in back arc side. Clear relationship is not found between the lateral variations of

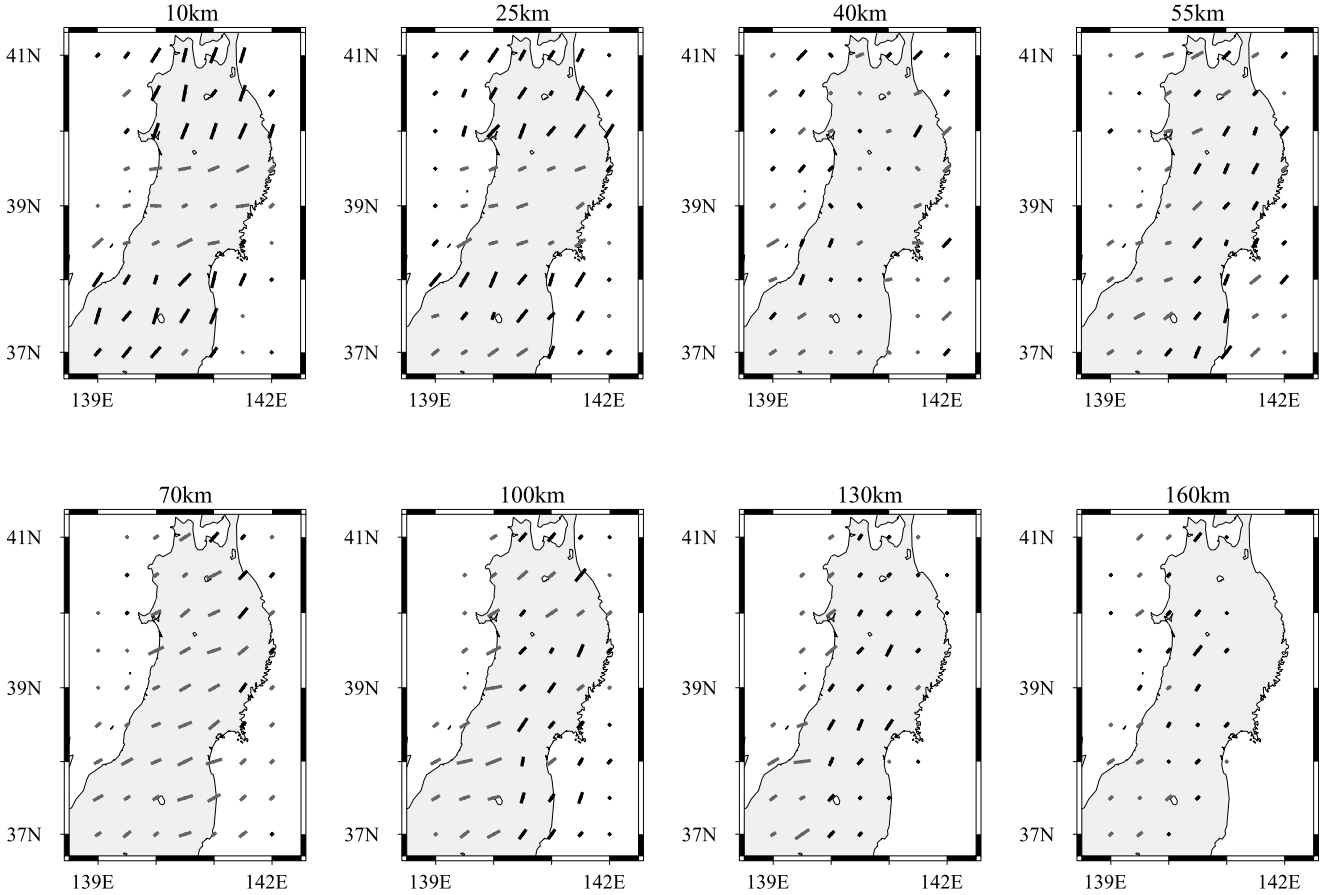

Figure 9. Map of anisotropic velocity perturbations estimated from the error-contaminated travel time data. See Figure 5 for symbols and perturbation scale.

the isotropic and anisotropic velocities. In the upper mantle, the E-W axis orientation is conspicuous at about 55 and 70 km depths, and a region of the N-S axis orientation appears at 70 km depth under the east coast. The region shifts toward the west with increasing depth, and the E-W axis orientation gradually disappears. This depth change in azimuthal anisotropy is consistent with 3-D heterogeneity of the isotropic velocity structure in which a high-velocity region migrates westward with increasing depth (Figure 10). Figure 13 depicts vertical cross section of the anisotropy direction along A–A′ line across the northeast Japan arc. The E-W axis orientation is predominant in the low-velocity mantle wedge and the N-S axis orientation is marked in the high-velocity Pacific slab. Thus we emphasize that the high-velocity Pacific slab has the azimuthally anisotropic property that P-wave velocity is high in N-S direction, while the low-velocity mantle wedge exhibits high velocity in E-W direction. These results are robust because the anisotropy structure does not change so much even if another initial set of model parameters is used for the 3-D velocity structure inversion.

[14] The relocated hypocenters and origin times are compared with their initial values. Table 1 lists the average and standard deviation of the source parameter changes obtained through the inversion. The source parameter changes are small so much. The 3-D heterogeneity of isotropic and anisotropic velocity structure has insignificant effect on the hypocenter determination of local earthquakes.

5. Discussion

[15] The 3-D variations of isotropic and anisotropic P-wave velocities were retrieved from the first P-arrival time data from local earthquakes in the Tohoku district, northeast Japan. We examine the validity of our estimate of the P-wave structure, comparing with the results of the shear-

Table 1. Average, Average Absolute Value, and Standard Deviation of the Source Parameter Changes[a]

	Case 1			Case 2			Real Inversion	
	Average	AA	SD	Average	AA	SD	Average	SD
Origin time, s	−0.02	0.16	0.11	−0.01	0.15	0.18	0.008	0.54
Latitude, km	−0.02	0.48	0.79	0.06	0.45	1.04	−0.37	3.14
Longitude, km	−0.11	0.47	0.60	−0.17	0.42	0.87	−0.40	3.78
Depth, km	−0.03	0.57	0.80	−0.01	0.53	1.20	−2.12	5.36

[a]Cases 1 and 2 show results from the error-free and the error-contaminated data. The two leftmost columns show results from the real data. AA, average absolute; SD, standard deviation.

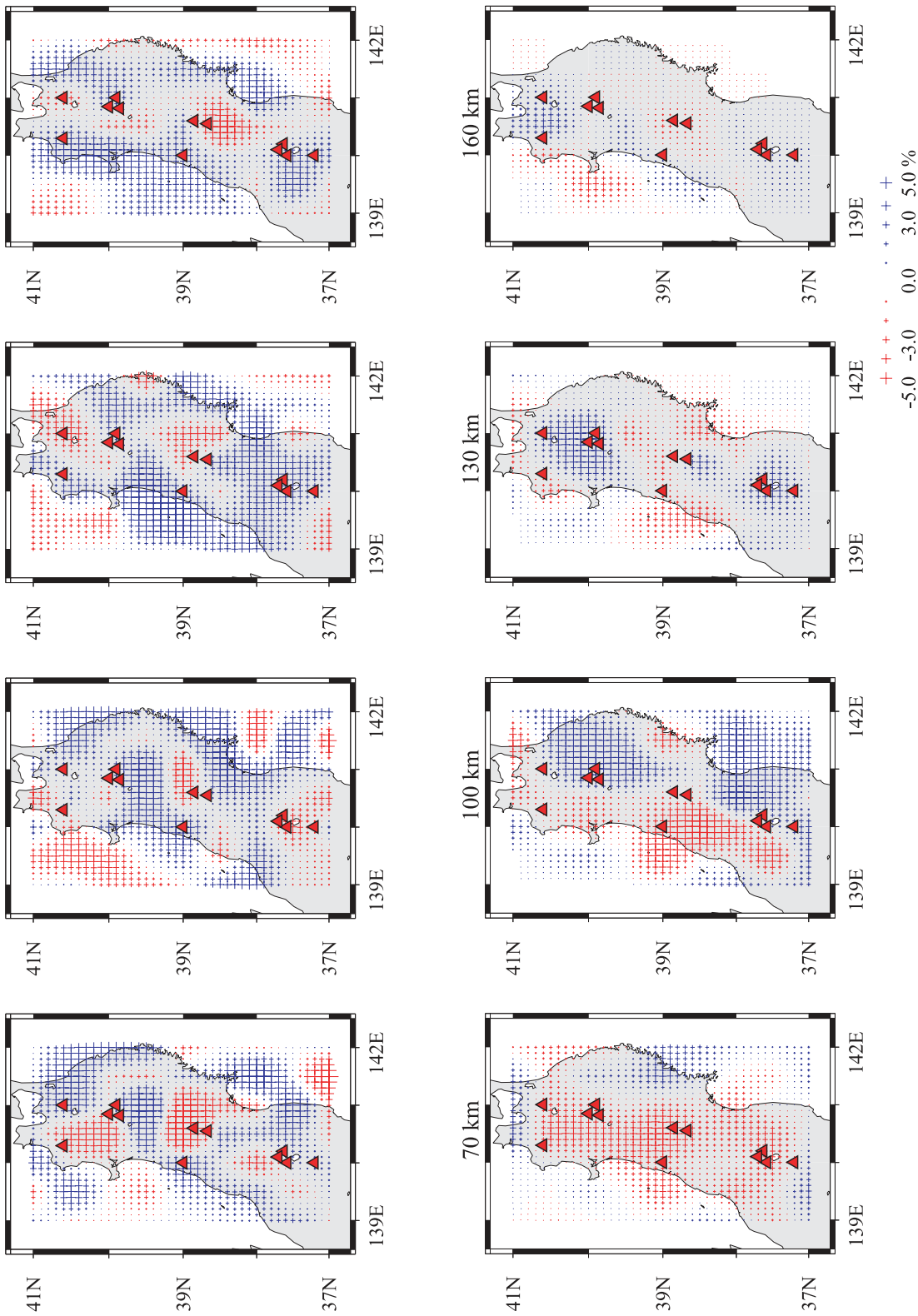

Figure 10. Lateral variations of isotropic velocity perturbations at different depths. Red and blue crosses represent low- and high-velocity perturbations, respectively. Triangles denote active volcanoes. The perturbation scale is shown in the bottom.

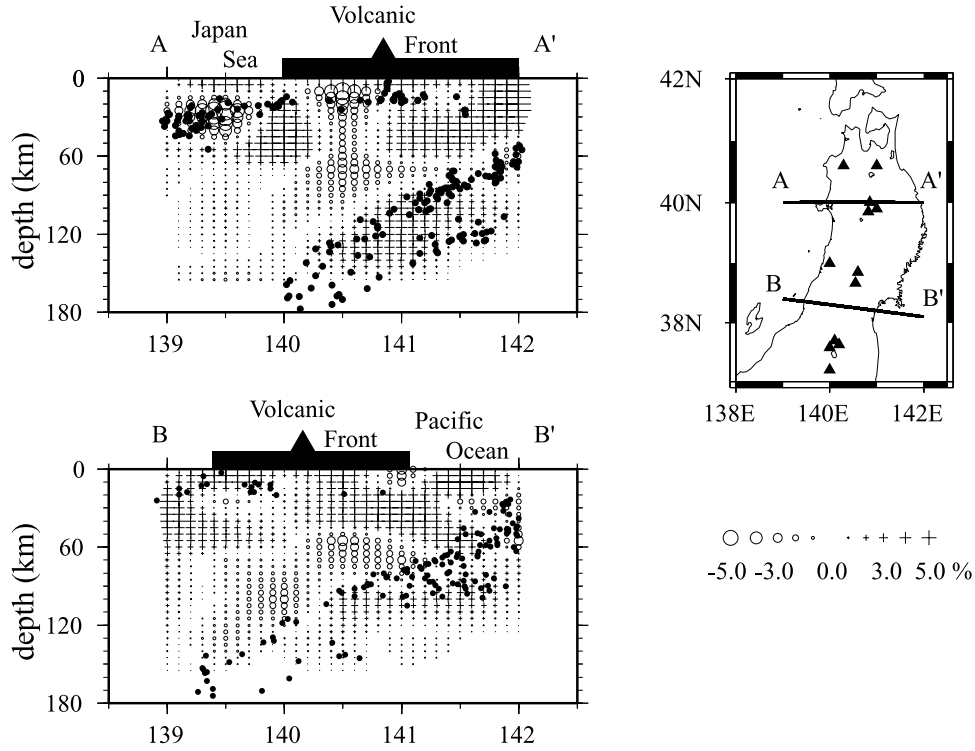

Figure 11. Vertical cross sections along A–A' and B–B′ lines of the 3-D isotropic velocity perturbation. Dots and triangles indicate earthquake hypocenters and active volcanoes, respectively. The perturbation scale is shown at bottom right.

wave splitting studies and other seismological studies, and then search for plausible factors that cause the seismic anisotropy in the crust and upper mantle.

5.1. Validity of the P-Wave Anisotropic Velocity Structure

[16] Figure 14 depicts the P-wave anisotropy structures at 0 and 10 km depths, along with the S-wave anisotropy structure [*Sakakibara et al.*, 2003] and trajectories of the maximum horizontal compression axes estimated by stress measurements of the crust [*Ando*, 1979]. In the shallow part of the crust, the fast propagation directions are nearly parallel to the maximum horizontal compression axes in E-W direction (Figure 14a). At about 10 km depth, they are also compatible with the fast polarization directions estimated from split shear waves of crustal earthquakes, especially in ellipse areas, the P- and S-wave anisotropy directions are in excellent agreement (see Figures 14b and 14c). It should be emphasized that the P-wave anisotropic structure, which was inferred from the P-wave arrival time data from deep-focus and intermediate-depth earthquakes as well as crustal earthquakes, is consistent with the polarization anomaly observations of shear waves from crustal earthquakes. This indicates that the first P-arrival time data have high resolution to estimate the seismic anisotropy structure as well as lateral heterogeneity of the isotropic velocity.

[17] In the upper mantle, the shear-wave splitting studies revealed that the fast polarizations in N-S and E-W directions are predominant in east and west sides of the Tohoku district, respectively [*Okada et al.*, 1995; *Nakajima and Hasegawa*, 2004]. The lateral variation supports our emphasis that the fast propagation axis of P-waves is in nearly E-W direction in the low-velocity mantle wedge of the west side of the same study area and in nearly N-S direction in the Pacific slab descending beneath the east side. Although in the inversion we used the arrival time data of P waves which travel through one or more anisotropic zones in the upper mantle and crust, the feature of the P-wave anisotropy structure is quite similar to that of the S-wave anisotropy structure inferred from the shear-wave splitting data. This consistency is also comprehensible from the conclusions of laboratory experiments that the fast polarization direction of split shear wave is parallel to the fast propagation axis of P-waves [e.g., *Crampin*, 1978; *Kasahara et al.*, 1968; *Zhang and Karato*, 1995]. These results indicate the validity of our estimates of the isotropic and anisotropic velocity structures. The inversion of the first P-arrival time data is a useful method for imaging 3-D variation of anisotropy velocity structure, as well as isotropic velocity structure, with high resolution.

5.2. Cause of P-Wave Anisotropy

[18] The anisotropy structure reveals that in the shallow part of the crust the fast propagation axes of P-waves are nearly parallel to trajectories of the maximum horizontal compression axes (Figure 14a). Thus the upper crust anisotropy is thought to be governed by local stress field. Laboratory experiments of rock mechanics showed that the P-wave velocity is higher in the cylindrical direction than in the radial direction when a cylindrical rock sample is subjected to uniaxial compression stress parallel to the cylindrical axis. This P-wave anisotropy was interpreted

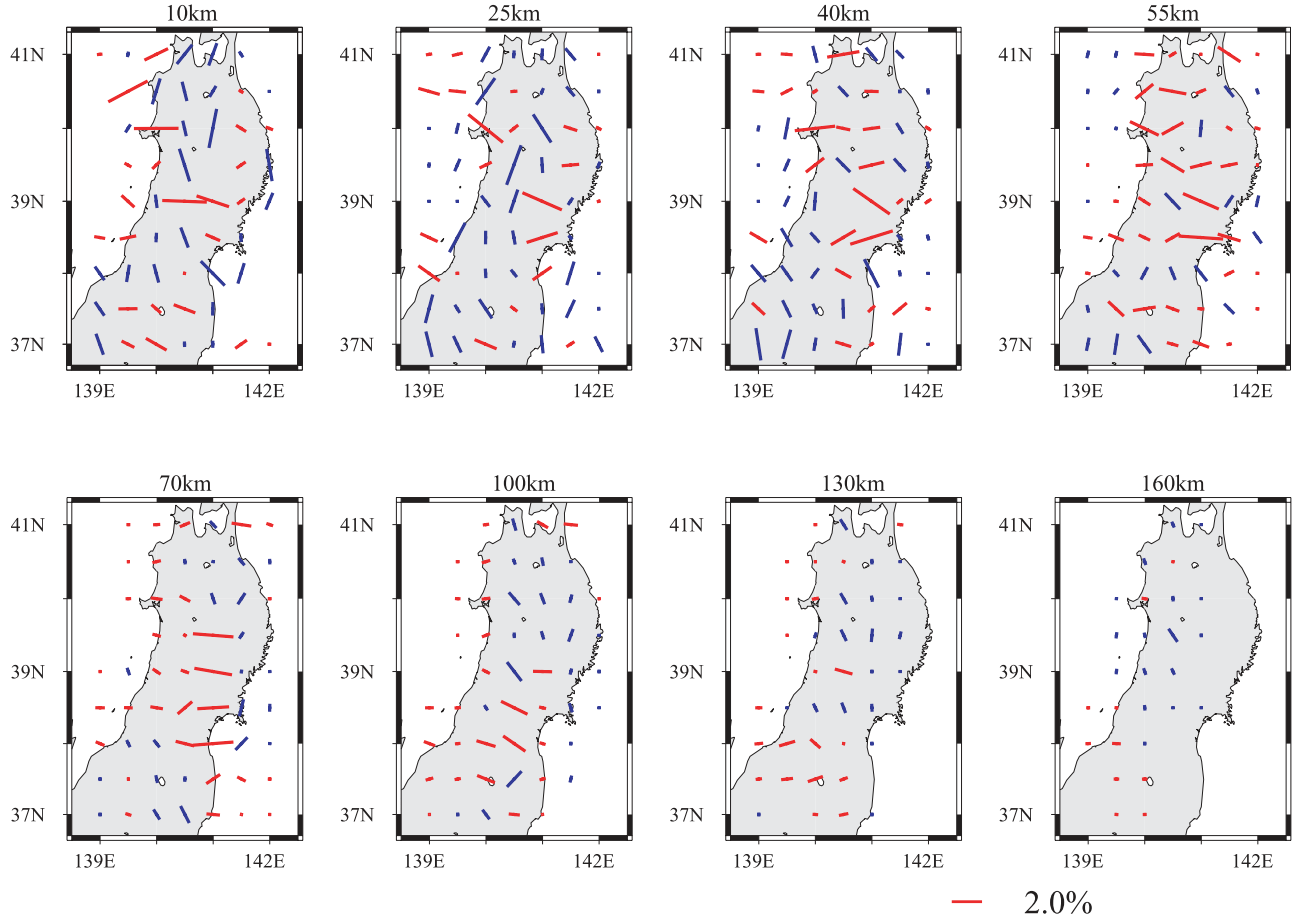

Figure 12. Lateral variations of anisotropic velocity perturbations. Length and azimuth of the bar indicate the anisotropy intensity and the fast propagation direction of P-waves, respectively. Red and blue bars indicate the fast propagation axes orientating from N45°E–S45°W to S45°E–N45°W and from N45°W–S45°E to N45°E–S45°W, respectively. The perturbation scale is shown at bottom.

as resulting from alignment of microcracks induced parallel to the compression stress direction [*Gupta*, 1973]. If the alignment of vertical microcracks arising from local stress field gives rise to the seismic anisotropy in the upper crust, as indicated by *Crampin* [1987], the laboratory experiments help us understand that P-waves exhibit the fast propagation in E-W direction which is the maximum horizontal compression direction in the Tohoku district.

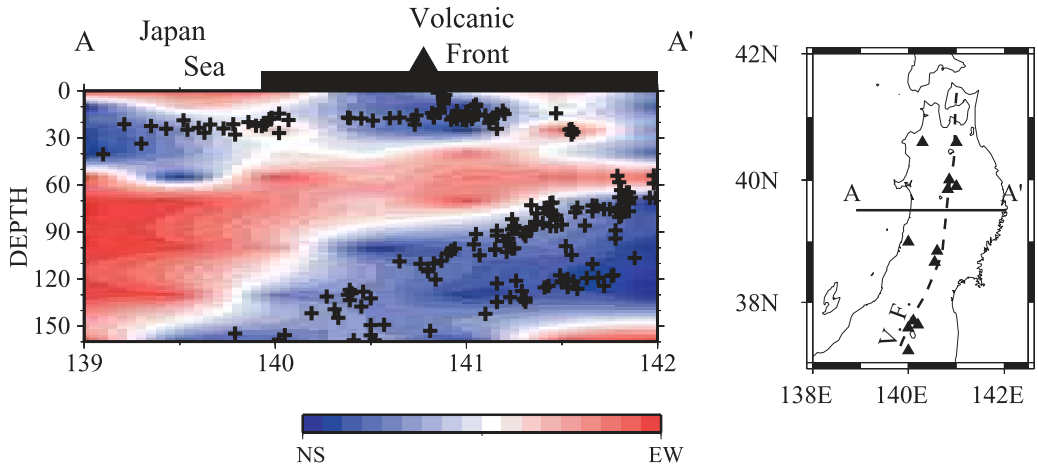

Figure 13. Vertical cross section along A–A′ line of the 3-D variation of the fast propagation direction of P-waves. Crosses indicate the earthquake hypocenters. Location of the profile line is shown in the right map, where dashed line shows the volcanic front (VF).

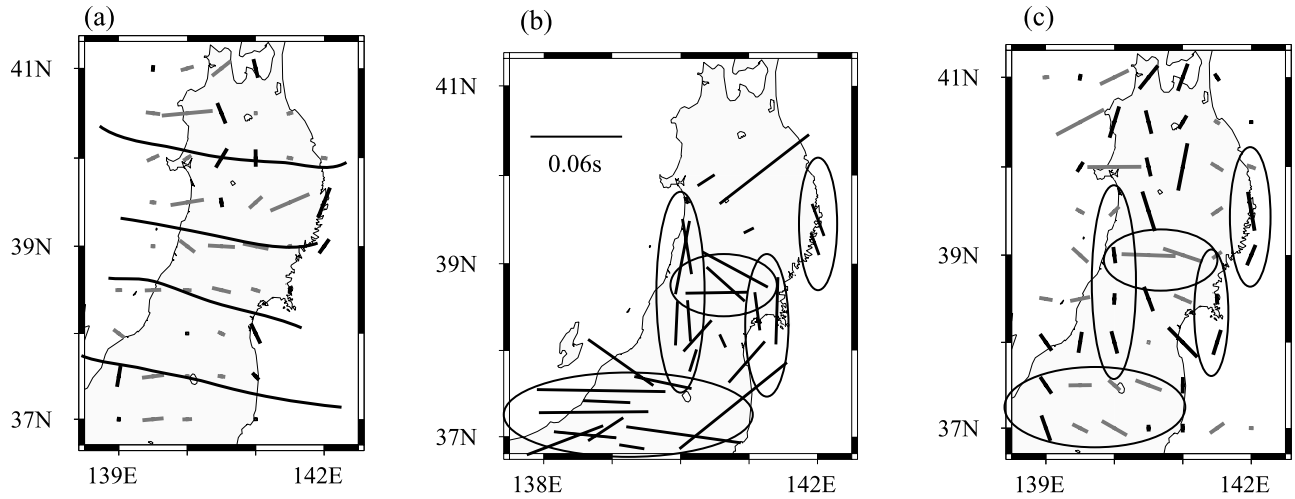

Figure 14. Comparisons of the P-wave anisotropy in the crust with other geophysical data: (a) the fast propagation directions (bar) of P-waves at 0-km depth and the trajectories of the maximum horizontal compression (solid curves) in the crust; (b) the fast polarization directions of the crust, as estimated by the shear-wave splitting study (modified from the original figure of *Sakakibara et al.* [2003]); and (c) the fast propagation directions of P-wave anisotropy at 10-km depth. Ellipse areas in Figures 14b and 14c are almost the same. See Figure 5 for an explanation of black and gray bars.

[19] In comparison with the P-wave anisotropy in the shallow crust, the deep crust shows more heterogeneous anisotropy structure. The fast propagation axes in E-W and N-S directions predominantly appear in the forearc and back arc sides of the volcanic front, respectively. This lateral variation of the axis orientation is quite similar to the distribution of the horizontal displacement velocities relative to the North American plate, which is calculated from the GPS data [*Sato et al.*, 2002]. The lower crust deformation has been thought to be more ductile because of the low seismic activity [*Sibson*, 1984]. If the lower crust is plastically deformed as the displacement velocity distribution calculated from the GPS data, the alignment of crust minerals might occur during the plastic flow deformation, leading to the P-wave anisotropy structure which is consistent with the GPS observation. Therefore the mineral alignment associated with the plastic deformation is interpreted as giving rise to the seismic anisotropy of the deep crust. A recent study of plate tectonics shows that the Tohoku district is positioned between the Pacific and Amurian plates [e.g., *Wei and Seno*, 1998; *Heki et al.*, 1999]. The forearc crust undergoes the ductile deformation in E-W direction caused by the Pacific plate moving westward, whereas the Amurian plate moving eastward [e.g., *Wei and Seno*, 1998; *Heki et al.*, 1999] may change the deformation direction of the back arc crust into N-S direction, interrupting the ductile deformation in E-W direction. Thus, if the mineral alignment along the plastic deformation is a plausible cause for the P-wave anisotropy of the deep crust, the difference between the anisotropy directions in forearc and back arc sides is interpreted as being due to the Amurian plate.

[20] We showed that the low-velocity mantle wedge above the high-velocity Pacific slab dipping toward the west has the seismic anisotropy that P-waves can propagate fast in nearly E-W direction. The mantle anisotropy has been mainly explained by two mechanisms. One is lattice-preferred orientation of the mantle minerals such as olivine that is the most abundant mineral in the upper mantle, and the other is alignment of inclusions filled with partially melted liquid. The former mechanism results from alignment of the mantle minerals in the direction of the mantle flow related to the present-day plate motion and subduction of oceanic slab. The flow direction induced by subduction of the oceanic plate is in agreement with the azimuth at which the plate descends [e.g., *Ribe*, 1989; *Furukawa*, 1993]. Since in the Tohoku district the subduction direction of the Pacific plate is in approximately the west, if the mantle anisotropy is formed by the lattice-preferred orientation of mantle minerals, we can easily understand that the fast propagation axis of azimuthal anisotropy is in E-W direction. The latter mechanism, alignment of partially melted inclusions, arises from the fact that the liquid-filled inclusions with small aspect ratio align parallel and/or subparallel to the maximum deviatoric compression stress in the partially melted mantle [*Nur and Simmons*, 1969; *Zimmerman et al.*, 1999]. The mantle wedge of the Tohoku district should be subject to the E-W compression in order to explain the mantle wedge anisotropy with the latter mechanism. However, the recent numerical simulations of stress state in the subduction zone predict the mantle wedge to undergo the compression stress in N-S direction [*Furukawa*, 1993; *Fischer et al.*, 2000]. This means that the partially melted inclusions cannot align in E-W direction, and thus the latter mechanism is inadequate to demonstrate a cause of the mantle wedge anisotropy. The lattice-preferred orientation of mantle minerals is preferable to the alignment of the melted inclusions for explaining the seismic anisotropy of the E-W axis orientation in the mantle wedge.

[21] It is well known that the oceanic plate under the ocean floor exhibits anisotropic property such that P-wave velocity becomes high when propagating in the direction of sea floor spreading [e.g., *Hess*, 1964]. Unfortunately, the

anisotropy of the oceanic slab that subducts beneath the island arcs or continents has never been observed by the polarization anomaly of shear waves and azimuthal variation of P-wave velocity. Nevertheless the seismic anisotropy in the Pacific slab was indirectly suggested from shear-wave splitting observed at seismic stations of the whole Japan islands [*Fukao*, 1984; *Hiramatsu et al.*, 1997]. We indicated that the Pacific slab descending beneath the Tohoku district has the anisotropic property that the fast propagation axes of P-waves are in nearly N-S direction. The slab anisotropy is consistent with the large-scale anisotropy of P-wave velocity under the ocean bottom, which was discovered by the explosion seismological experiments in the northwest Pacific basin [*Shimamura*, 1984]. In addition, the N-S fast direction is nearly perpendicular to the magnetic lineation that *Isezaki and Miki* [1978] found in the Pacific plate extending over the ocean bottom. Therefore the P-wave anisotropy of the Pacific slab beneath the Tohoku district can be interpreted as being frozen after the Pacific plate formed, while the mantle-wedge anisotropy is generated by present-day mantle convection. The Pacific slab is descending beneath the Tohoku district, preserving the original anisotropy that the Pacific plate gained when it formed 130 Myr ago.

6. Conclusions

[22] The 3-D variations of isotropic and anisotropic velocity structures were retrieved from the first P-arrival time data from local earthquakes in the Tohoku district, northeast Japan. The P-wave anisotropy was modeled by weak azimuthal anisotropy which is caused by hexagonal symmetry axes distributed horizontally. In spite of no assumption of high-velocity oceanic slab in initial velocity model, the high-velocity Pacific slab dipping toward the west was clearly imaged in the retrieved isotropic velocity structure. The high-velocity slab was continuously traced from 55 km depth down to 130 km depth, and in good agreement with the seismic belt which the deep-focus and intermediate-depth earthquakes delineate. Intensive low-velocity anomaly regions were found in the mantle wedge just above the Pacific slab. They were distributed nearly parallel to the upper boundary of the Pacific slab and connected to the magma reservoirs just below the active volcanoes. These features of the isotropic velocity structure were not much different from those of previous studies, although the seismic anisotropy was taken into account in the inversion of P-arrival time data.

[23] On the other hand, the anisotropy structure shows several features. The fast propagation axes of P-waves were in nearly E-W direction in shallow part of the crust and parallel to the trajectories of the maximum horizontal compression axes estimated by stress measurements of the crust. In the deep crust below 10 km depth, the fast propagation axis was predominantly orientated in E-W and N-S directions in the forearc and back arc sides of the volcanic front, respectively. The low-velocity mantle wedge has the azimuthal anisotropy that the fast propagation axis of P-waves was in nearly E-W direction, while the high-velocity Pacific slab exhibits the anisotropy to be fast propagation in N-S direction. In particular, the slab anisotropy appeared at 70 km depth under the east coast of the Tohoku district and could be traced with increasing depth down to 160 km under the west coast of the district, as the subduction of the high-velocity slab was imaged in the 3-D structure of isotropic P-wave velocity. These features of P-wave anisotropy structure were in good agreement with the regional variations of the fast polarization directions measured by shear-waves splitting observations.

[24] The upper crust anisotropy was attributed to alignment of vertical microcracks induced by the regional tectonic stress field, because the fast propagation axes of azimuthal anisotropy were parallel to the maximum compression axis of the crust. The lower crust anisotropy was interpreted as being due to alignment of the crust minerals along plastic flow of the lower crust, which is induced by the interaction between the Pacific and Amurian plates. The fast propagation directions of P-waves in the mantle wedge were almost coincident with the subduction direction of the Pacific slab, and the fast anisotropy direction in the subducting slab was nearly perpendicular to the magnetic lineation of the Pacific plate in the northwest Pacific. Therefore we reached the conclusion that the mantle anisotropy is attributed to present-day mantle process such as the mantle wedge convection and the plate motion, while the slab anisotropy is the original anisotropic property gained when the Pacific plate formed.

Appendix A

[25] Here we derive equation (1) in the text, following *Hirahara and Ishikawa* [1984]. We define elastic parameters $\Gamma_{ijkl} = C_{ijkl}/\rho$, where C_{ijkl} and ρ denote the elastic tensor and density of anisotropic medium, respectively. In the case of nearly isotropic medium, the elastic parameters are written as,

$$\Gamma_{ijkl} = \Gamma^0_{ijkl} + \gamma_{ijkl}, \tag{A1}$$

where Γ^0_{ijkl} and γ_{ijkl} are the elastic parameters of unperturbed isotropic medium and their small perturbations representing the anisotropy of the medium, respectively. According to *Backus* [1965], the P-wave velocity in the weakly anisotropic medium is expressed as

$$v^2 = c^2 + B^{(1)} + O\left(\gamma^2_{ijkl}\right) \tag{A2}$$

$$B^{(1)} = \gamma_{ijkl}\nu_i\nu_j\nu_k\nu_l, \tag{A3}$$

where c is the P-wave velocity in the isotropic medium and (ν_1, ν_2, ν_3) represents the direction cosine of a unit P-wave propagation vector. In (A3), the Einstein summation convection is assumed for the repeated indices. Using small perturbation Δv_{iso} to the isotropic velocity v_0, we write the isotropic P-wave velocity as

$$c = v_0\left(1 + \frac{\Delta v_{iso}}{v_0}\right). \tag{A4}$$

The second-order terms $O(\gamma^2_{ijkl})$ in (A2) are usually negligibly small [cf. *Backus*, 1982; *Crampin*, 1982].

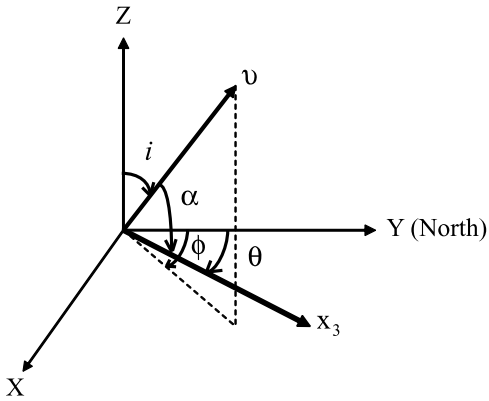

Figure A1. System of the coordinate specifying ray path and the symmetry axis. Here ν is the unit propagation vector of ray with incident angle i and azimuthal angle ϕ;. x_3 is the hexagonal symmetry axis in the horizontal plane with azimuth angle θ; and α is the angle between the ray direction and the hexagonal symmetry axis.

Introducing (A4) into (A2), we obtain the anisotropic velocity perturbation $\Delta v = v - v_0$ to the isotropic velocity v_0

$$\frac{\Delta v}{v_0} = \frac{\Delta v_{iso}}{v_0} + \frac{1}{2v_0^2} B^{(1)}, \tag{A5}$$

where $O(\gamma_{ijkl}^2)$ and higher-order terms of the velocity perturbations $B^{(1)}$ and Δv_{iso} are neglected.

[26] In the case where elasticity of an anisotropic medium is hexagonally symmetric around the x_3-axis, nonzero elastic parameters are

$$\begin{aligned}
&\gamma_{1111} = \gamma_{2222}, \gamma_{3333},\\
&\gamma_{1122}, \gamma_{1133} = \gamma_{2233}, \gamma_{1313} = \gamma_{2323},\\
&\gamma_{1212} = \frac{1}{2}(\gamma_{1111} - \gamma_{1122}).
\end{aligned}$$

Substitution of the elastic parameters into (A3) with the aid of $\nu_1^2 + \nu_2^2 + \nu_3^2 = 1$ yields

$$\begin{aligned}
B^{(1)} &= \gamma_{1111} + 2(\gamma_{1133} + 2\gamma_{1313} - \gamma_{1111})\nu_3^2\\
&\quad + \{\gamma_{1111} + \gamma_{3333} - 2(\gamma_{1133} + 2\gamma_{1313})\}\nu_3^4\\
&= A_1 + B_1 \cos 2\alpha + E_1 \cos 4\alpha,
\end{aligned} \tag{A6}$$

where α denotes the angle between the propagation direction and the symmetry axis (see Figure A1) and

$$\begin{aligned}
A_1 &= \frac{1}{8}\{3(\gamma_{1111} + \gamma_{3333}) + 2(\gamma_{1133} + 2\gamma_{1313})\}\\
B_1 &= \frac{1}{2}(\gamma_{3333} - \gamma_{1111})\\
E_1 &= \frac{1}{8}\{\gamma_{1111} + \gamma_{3333} - 2(\gamma_{1133} + 2\gamma_{1313})\}.
\end{aligned}$$

From (A5) and (A6), we obtain

$$\frac{\Delta v}{v_0} = A_1' + B_1' \cos 2\alpha + E_1' \cos 4\alpha, \tag{A7}$$

where

$$\begin{aligned}
A_1' &= \frac{1}{2v_0^2}(2v_0 \Delta v_{iso} + A_1)\\
B_1' &= \frac{1}{2v_0} B_1\\
E_1' &= \frac{1}{2v_0} E_1.
\end{aligned}$$

When the P-waves propagate into the anisotropic medium where the hexagonal symmetry axis is in the horizontal plane (see Figure A1), the angle α between the hexagonal axis and the propagation direction is written as

$$\cos\alpha = \sin i \sin\phi \sin\theta + \sin i \cos\phi \cos\theta, \tag{A8}$$

where i and ϕ are the incident angle and azimuth of the ray path and θ is azimuth of the hexagonal symmetry axis. The azimuthal angles ϕ and θ are measured clockwise from the north. Observations of azimuthal variations of the P_n velocity suggested that in the upper mantle the cos 4α term is negligibly small in comparison with other terms [e.g., *Raitt et al.*, 1969]. Introducing (A8) into (A7) and neglecting the cos 4α term, we finally obtain the same expression as equation (1) in the text

$$\frac{\Delta v}{v_0} = A + B \sin^2 i\{1 + \cos 2(\phi - \theta)\}, \tag{A9}$$

where

$$\begin{aligned}
A &= \frac{1}{2v_0^2}\left[2v_0 \Delta v_{iso} + \frac{1}{8}\{7\gamma_{1111} - \gamma_{3333} + 2(\gamma_{1133} + 2\gamma_{1313})\}\right]\\
B &= \frac{1}{4v_0^2}(\gamma_{3333} - \gamma_{1111}).
\end{aligned}$$

[27] **Acknowledgments.** We thank the Earthquake Information Center of Tokyo University for providing the P-arrival time data. Critical comments from Martin Rayners, Junichi Nakajima, an anonymous reviewer, and an anonymous associate editor were useful for revising the manuscript. This study was supported by grant-in-aid for Scientific Research (C) (12640409) of the Ministry of Education, Culture, Sports, Science and Technology. All the figures are drawn using GMT [*Wessel and Smith*, 1991].

References

Ando, M. (1979), The stress field of the Japan islands in the last 0.5 million years (in Japanese), *Earth Mom. Symp.*, *7*, 541–546.

Ando, M., Y. Ishikawa, and H. Wada (1980), S-wave anisotropy in the upper mantle under a volcanic area in Japan, *Nature*, *286*, 43–46.

Ando, M., Y. Ishikawa, and F. Yamazaki (1983), Shear wave polarization anisotropy in the upper mantle beneath Honshu, *J. Geophys. Res.*, *88*, 5850–5864.

Audoine, E., M. K. Savege, and K. Gledhill (2000), Seismic anisotropy from local earthquakes in the transition region from a subduction to a strike-slip plate boundary, New Zealand, *J. Geophys. Res.*, *105*, 8013–8033.

Backus, G. E. (1965), Possible forms of seismic anisotropy of the uppermost mantle under oceans, *J. Geophys. Res.*, *70*, 3429–3439.

Backus, G. E. (1982), Reply: Limits of validity of first-order perturbation theory for quasi-P velocity in weakly anisotropic media, *J. Geophys. Res.*, *87*, 4641–4644.

Cara, M., and J. J. Leveque (1988), Anisotropy of the asthenosphere: The higher-mode data of the Pacific revised, *Geophys. Res. Lett.*, *15*, 205–208.

Cerveny, V. (1972), Seismic rays and ray intensities in inhomogeneous anisotropic media, *Geophys. J. R. Astron. Soc.*, *29*, 1–13.

Chen, C.-H., Y.-H. Chen, H.-Y. Yen, and G.-K. Yu (2003), Lateral variation of Pn velocity and anisotropy in Taiwan from travel-time tomography, *Earth Planets Space*, *55*, 223–230.

Christensen, N. I. (1984), The magnitude, symmetry and origin of upper-mantle anisotropy based on fabric analyses of ultramafic tectonics, *Geophys. J. R. Astron. Soc.*, *76*, 89–111.

Crampin, S. (1978), Seismic wave propagation through a cracked solid: Polarization as a possible dilatancy diagnostic, *Geophys. J. R. Astron. Soc.*, *53*, 467–496.

Crampin, S. (1982), Comments on 'possible forms of anisotropy of the uppermost mantle under the oceans' by George E. Backus, *J. Geophys. Res.*, *87*, 4636–4640.

Crampin, S. (1987), Geological and industrial implications of extensive-dilatancy anisotropy, *Nature*, *328*, 491–496.

Eberhart-Phillips, D., and C. M. Henderson (2004), Including anisotropy in 3-D velocity inversion and application to Marlborough, New Zealand, *Geophys. J. Int.*, *156*, 237–254, doi:10.1046/j.1365-246X.2003.02044.x.

Fischer, K. M., E. M. Parmentier, A. R. Stine, and E. R. Wolf (2000), Modeling anisotropy and plate-driven flow in the Tonga subduction back arc, *J. Geophys. Res.*, *105*, 16,181–16,191.

Fukao, Y. (1984), Evidence from core-reflected shear-waves for anisotropy in the Earth's mantle, *Nature*, *309*, 695–698.

Furukawa, Y. (1993), Magmatic processes under arc and formulation of the volcanic front, *J. Geophys. Res.*, *98*, 8309–8319.

Gupta, I. N. (1973), Seismic velocities in rock subjected to axial loading up to shear fracture, *J. Geophys. Res.*, *78*, 6936–6942.

Hamada, N. (1984), Re-examination of travel time tables for local earthquakes (in Japanese), *Pap. Meteorol. Geophys.*, *35*, 109–167.

Hasemi, A., H. Ishii, and A. Takagi (1984), Fine structure beneath the Tohoku District, northeastern Japan arc, as derived by an inversion of P-wave arrival times from local earthquakes, *Tectonophysics*, *101*, 245–265.

Hearn, T. M. (1996), Anisotropic *Pn* tomography in the western United States, *J. Geophys. Res.*, *101*, 8403–8414.

Heki, K., S. Miyazaki, T. Takahashi, M. Kasahara, F. Kimata, S. Miura, N. F. Vasolenko, A. Ivashchenko, and K. An (1999), The Amurian Plate motion and current plate kinetics in eastern Asia, *J. Geophys. Res.*, *104*, 29,147–29,155.

Hess, H. H. (1964), Seismic anisotropy of the uppermost mantle under oceans, *Nature*, *203*, 629–631.

Hirahara, K., and Y. Ishikawa (1984), Travel time inversion for three-dimensional P-wave velocity anisotropy, *J. Phys. Earth*, *32*, 197–218.

Hiramatsu, H., M. Ando, and Y. Ishikawa (1997), ScS wave splitting of deep earthquakes around Japan, *Geophys. J. Int.*, *128*, 409–424.

Hiramatsu, H., M. Ando, T. Tsukuda, and T. Ooida (1998), Three-dimensional image of the anisotropic bodies beneath central Honshu, Japan, *Geophys. J. Int.*, *135*, 801–816.

Ichikawa, M., and E. Mochizuki (1971), Travel time tables for local earthquakes in and near Japan (in Japanese), *Pap. Meteorol. Geophys.*, *22*, 229–290.

Isezaki, N., and H. Miki (1978), Compilation of magnetic data in the northwestern Pacific and in the Philippine Sea, *J. Phys. Earth*, *26*, S403–S407, suppl..

Ishise, M., and H. Oda (2002), The Philippine Sea plate examined based on the basis of P-wave anisotropy, Nakanishi, I., 277 pp., Kyoto Univ., Kyoto, Japan.

Kaneshima, S. (1990), Origin of crustal anisotropy: Shear wave splitting studies in Japan, *J. Geophys. Res.*, *95*, 11,121–11,133.

Karato, S., and P. Wu (1993), Rheology of the upper mantle: A synthesis, *Science*, *260*, 771–778.

Kasahara, J., I. Suzuki, and M. Kumazawa (1968), Plane and spherical wave velocities and energy flow in anisotropic media, *J. Seism. Soc. Jpn.*, *21*, 282–292.

Kirkwood, S. C., and S. Crampin (1981), Surface-wave propagation in an ocean basin with an anisotropic upper mantle: Observations of polarization anomalies, *Geophys. J. R. Astron. Soc.*, *64*, 487–497.

McKenzie, D. (1979), Finite deformation during fluid flow, *Geophys. J. R. Astron. Soc.*, *58*, 689–715.

Nakajima, J., and A. Hasegawa (2004), Shear-wave polarization anisotropy and subduction-induced flow in the mantle wedge of northeastern Japan, *Earth Planet. Sci. Lett.*, *225*, 365–377, doi:10.1016/j.epsl.2004.06.011.

Nakajima, J., T. Matsuzawa, A. Hasegawa, and D. Zhao (2001), Three-dimensional structure of Vp, Vs, and Vp/Vs beneath northeastern Japan: Implications for arc magmatism and fluids, *J. Geophys. Res.*, *106*, 21,843–21,857.

Nur, A., and G. Simmons (1969), Stress-induced velocity anisotropy in rock: An experimental study, *J. Geophys. Res.*, *74*, 6667–6674.

Oda, H., and H. Shimizu (1997), S wave splitting observed in southwest Japan, *Tectonophysics*, *270*, 73–82.

Okada, T., T. Matsuzawa, and A. Hasegawa (1995), Shear-wave polarization anisotropy beneath the north-eastern part of Honshu, Japan, *Geophys. J. Int.*, *123*, 781–797.

Park, J., and Y. Yu (1992), Anisotropy and coupled free oscillations: Simplified models and surface wave observations, *J. Geophys. Int.*, *110*, 401–420.

Raitt, R. W., G. G. Shor, T. J. G. Francis, and G. B. Morris (1969), Anisotropy of the Pacific upper mantle, *J. Geophys. Res.*, *74*, 3095–9109.

Ribe, N. M. (1989), Seismic anisotropy and mantle flow, *J. Geophys. Res.*, *97*, 3429–3439.

Sakakibara, Y., K. Tadokoro, and K. Hirahara (2003), A nation wide anisotropy distribution in the upper crust using shear-wave splitting by the use of Hi-net data, paper presented at Fall Meeting, Seismol. Soc. Jpn., Kyoto, Japan.

Sato, T., S. Miura, K. Tachibana, Y. Satake, and A. Hasegawa (2002), Crustal deformation around Ou Backbone Range, northeastern Japan observed by dense GPS network, *J. Seism. Soc. Jpn.*, *55*, 181–191.

Savage, M. K. (1999), Seismic anisotropy and mantle deformation: What have we learned from shear wave splitting?, *Rev. Geophys.*, *37*, 65–106.

Sclater, J. G., B. Parsons, and C. Jaupart (1981), Oceans and continents: Similarities and differences in the mechanisms of heat loss, *J. Geophys. Res.*, *86*, 11,535–11,552.

Shearer, P. M., and C. H. Champman (1988), Ray tracing in anisotropic media with a linear gradient, *Geophys. J.*, *94*, 575–580.

Shimamura, H. (1984), Anisotropy in the oceanic lithosphere of the Northwestern Pacific Basin, *Geophys. J. R. Astron. Soc.*, *76*, 253–260.

Sibson, R. H. (1984), Roughness at the base of the seismogenic zone, *J. Geophys. Res.*, *89*, 8737–8747.

Thurber, C. H. (1983), Earthquake location and three-dimensional crustal structure in the Coyote Lake area, central California, *J. Geophys. Res.*, *88*, 8226–8236.

Thurber, C. H. (1992), Hypocenter-velocity structure coupling in local earthquake tomography, *Phys. Earth Planet Inter.*, *75*, 55–62.

Um, J., and C. Thurber (1987), A fast algorithm for two-point seismic ray tracing, *Bull. Seismol. Soc. Am.*, *77*, 972–986.

Wei, D., and T. Seno (1998), Determination of the Amurian plate motion, in *Mantle Dynamics and Plate Interactions in East Asia*, *Geodyn. Ser.*, vol. 27, edited by M. F. J. Flower et al., pp. 337–346, AGU, Washington, D. C.

Wessel, P., and W. H. F. Smith (1991), Free software helps map and display data, *Eos Trans. AGU*, *72*, 441–446.

Wolfe, C. J., and S. C. Solomon (1998), Shear-wave splitting and implication for mantle flow beneath the MELT region on the east Pacific rise, *Science*, *280*, 1230–1232.

Zhang, H., C. H. Thurber, D. Shelly, S. Ide, G. C. Beroza, and A. Hasegawa (2004), High-resolution subducting-slab structure beneath northern Honshu, Japan, revealed by double-difference tomography, *Geology*, *32*, 361–364, doi:10.1130/G20261.1.

Zhang, S., and S. Karato (1995), Lattice preferred orientation of olivine aggregates deformation in simple shear, *Nature*, *260*, 774–778.

Zhao, D., and A. Hasegawa (1993), P-wave tomographic imaging of the crust and upper mantle beneath the Japan islands, *J. Geophys. Res.*, *98*, 4333–4353.

Zhao, D., A. Hasegawa, and S. Horiuchi (1992), Tomographic imaging of P and S wave velocity structure beneath northeastern Japan, *J. Geophys. Res.*, *97*, 19,909–19,928.

Zimmerman, M. E., S. Zhang, and D. L. Kohlstedt (1999), Melt distribution in mantle rock deformed in shear, *Geophys. Res. Lett.*, *26*, 1505–1508.

M. Ishise and H. Oda, Department of Earth Sciences, Okayama University, 3-11 Tsushima Naka, Okayama 700-8530, Japan. (lfee0688@cc.okayama-u.ac.jp)